PERGAMON

International Journal of Non-Linear Mechanics 38 (2003) 767–779

INTERNATIONAL JOURNAL OF
NON-LINEAR MECHANICS

www.elsevier.com/locate/ijnonlinmec

# Non-linear dynamics of a stochastically excited beam system with impact

N. van de Wouw *, A. de Kraker, D.H. van Campen, H. Nijmeijer

*Department of Mechanical Engineering, Eindhoven University of Technology, P.O. Box 513, 5600 MB Eindhoven, The Netherlands*

**Abstract**

The response of non-linear, dynamic systems to stochastic excitation exhibits many interesting characteristics. In this paper, a strongly non-linear beam-impact system under both broad- and small-banded, Gaussian noise excitations is investigated. The response of this system is investigated both numerically, through a multi-degree-of-freedom model, and experimentally focusing on frequency-domain phenomena such as stochastic equivalents of harmonic and subharmonic solutions. An improved understanding of these stochastic response characteristics is obtained by comparing these to non-linear periodic response features of the system. It will be shown that in modelling such a continuous, linear system with a local non-linearity, the linear part can be effectively reduced to a description based on several modes. Combining this reduced, linear part with the local non-linearity in a reduced, non-linear model is shown to result in a non-linear model, which can be used to accurately predict the stochastic response characteristics of the original, continuous, non-linear system. It is shown that including more modes to the model causes its response to differ significantly from that of a single-degree-of-freedom model and show a better correspondence with experimental results, also in the frequency range of the first mode. 

## 1. Introduction

Non-linear, dynamic systems forced by random excitations are often encountered in practice. The source of randomness can vary from surface randomness in vehicle motion, environmental changes, such as earthquakes and wind exciting high rise buildings or wave motions at sea exciting offshore structures or ships, to electric or acoustic noise exciting mechanical structures. Often these stochastic excitations exhibit a coloured frequency spectrum. Moreover, many practical, non-linear systems comprise a continuous linear part and a local non-linearity.

In this paper, a system, representative for the class of systems mentioned above, namely, a base-excited beam system with a non-linear elastic stop is investigated. Systems with elastic stops are typical examples of systems with local non-linearities and represent a wide range of practical non-linear dynamic systems. Examples are gear rattle, ships colliding against fenders and snubbers in solar panels on satellites. Although the non-linearity is local, the dynamic behaviour of the entire system is influenced by it. Non-linear periodic response phenomena of these kind of systems have been studied extensively, see Refs. [1–4]. Moreover, a study of the stochastic response characteristics of a single-degree-of-freedom (SDOF) model of this system can be found in [5].

When stochastic excitations are applied to the non-linear beam system, it features many interesting,

* Corresponding author. Tel.: +31-40-2473358; fax: +31-40-2461418.
*E-mail address:* n.v.d.wouw@tue.nl (N. van de Wouw).

0020-7462/03/$ - see front matter 
PII: S0020-7462(01)00132-9

stochastic, non-linear response phenomena. These phenomena are of specific interest because they shed light on the common characteristics of periodic and stochastic dynamic behaviour. As a consequence, the behaviour of the system can be understood more thoroughly. The stochastic non-linear response phenomena will be studied numerically as well as experimentally. For the numerical investigations a model is used, in which the linear, continuous part of the system (the elastic beam) is reduced to a multiple-mode description. It will be shown that the model obtained by the reduction of the linear, continuous part of the system (the elastic beam) based on a limited number of elastic modes can accurately describe the stochastic response of the experimental system. A comparison of numerical and experimental results will display the added value of the multiple-degree-of-freedom (MDOF) model when compared with a SDOF model [5]. Herein, the applied, stochastic excitations are Gaussian and have a limited frequency band power spectral density. Still, these excitations can be broad- or narrow-banded processes. It should be noted that, particularly, the non-linear phenomena in the power spectral density of the response will be investigated extensively.

In the next section, we introduce the non-linear dynamic system and its two-degree-of-freedom (2DOF) model. In Section 3, a brief survey of simulated periodic response characteristics will be given. In Section 4, the simulation approach for stochastic excitations will be treated and the related simulation results will be discussed in Section 5. In Section 6, we present the experimental set-up. Furthermore, in Section 7, the simulation results are compared to the experimental results. Finally, in Section 8, we present some conclusions.

## 2. The non-linear beam system

### 2.1. System description

The non-linear, dynamic system comprises a linear elastic beam, which is clamped onto a rigid frame, and an elastic stop, see Fig. 1. The elastic stop consists of two ptfe (Teflon) half-spheres. The system is excited by a prescribed, stochastic displacement $y(t)$ of the rigid frame. The response $x(z,t)$ is the vertical displacement of the beam at the horizontal coordinate $z$. Firstly, in Section 2.2, the approach in building a MDOF model for the elastic beam will be illuminated. Next, in Section 2.3, a model for the elastic stop will be presented. The estimation of the parameters, describing the non-linearity, is based on experiments and will be elucidated in that section. Finally, in Section 2.4, a non-linear, 2DOF model of the beam-impact system will be discussed.

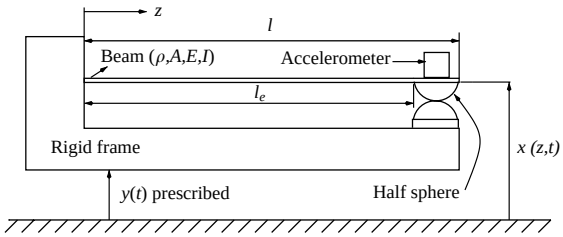


Fig. 1. The non-linear, base-excited beam system with Young's modulus $E = 1.9 \times 10^{11}$ N/mm$^2$, density $\rho = 8000$ kg/m$^3$, cross-section $A = 58.3$ mm$^2$, second moment of area of the cross-section $I = 18.5$ mm$^4$, length $l = 259.9$ mm ($l_e = 229$ mm), mass of a half-sphere $m_s = 12.4 \times 10^{-3}$ kg and mass of the accelerometer $m_a = 13.0 \times 10^{-3}$ kg.

### 2.2. Modelling the elastic beam

For the elastic beam, shear effects and rotational inertia will be neglected (Euler beam). In a first step, spatially discretized models for such a continuous system can be derived using the Rayleigh–Ritz method [6]. This method was applied to obtain a 4DOF model of the elastic beam, where the half-sphere and the accelerometer have been modelled as rigid parts at $z = (l + l_e)/2$. Note here that $l_e = l - 2R_s$, where $R_s$ is the radius of the half-sphere. Additional evaluations showed that a reduction of the 4DOF model to a model incorporating only the two modes corresponding to the lowest two eigenfrequencies is very acceptable with respect to our research goal. Moreover, these eigenfrequencies match their experimental equivalents quite well, see Table 1. Therefore, the 4DOF model was reduced to a 2DOF model using only these first two eigenmodes of the 4DOF model [7]. In Fig. 2, the modes corresponding to these eigenfrequencies are displayed. Moreover, corresponding dimensionless damping parameters are given, which were estimated by experimental means.

Table 1
Lowest two eigenfrequencies of the 4DOF model vs. experimental eigenfrequencies

| Eigenfrequencies (rad/s) | |
|---|---|
| Experimental | Model |
| 101.5 | 109.1 |
| 781.6 | 790.7 |

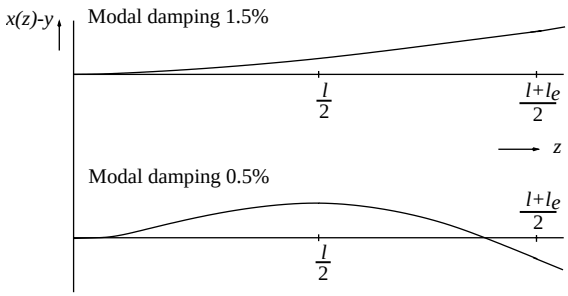


Fig. 2. Modes shapes and modal damping parameters corresponding to the lowest two eigenfrequencies.

### 2.3. Modelling the elastic stop

Here, the contact phenomenon will be modelled as a 'soft' impact, indicating that the deformation of the half-spheres during impact will be taken into account. Herein, the contact force will depend on the deformation (and deformation velocity) in a smooth fashion.

The elastic stop is modelled using a Hertzian contact model [8,9]. Using the Hertzian model, the following relationship holds between the contact force $F$ and the relative displacement of the two colliding spheres $\delta = y - x(z = l + l_e/2)$:

$$F = \tfrac{2}{3} E_r \sqrt{R_r}\,\delta^{1.5} = K_{\text{Hertz}}\delta^{1.5} \quad \text{for } \delta \geqslant 0. \tag{1}$$

In Eq. (1), the reduced Young's modulus $E_r$ reflects the material properties of both the colliding bodies. Furthermore, the reduced radius of curvature $R_r$ reflects the geometrical properties of the colliding bodies. These parameters are defined as

$$E_r = \frac{2}{(1-\nu_1^2)/E_1 + (1-\nu_2^2)/E_2}, \quad R_r = \frac{R_1 R_2}{R_1 + R_2}, \tag{2}$$

where $R_i$ is the principal radius of curvature of body $i$, while $E_i$ is the Young's modulus of body $i$ and $\nu_i$ the Poisson's ratio of body $i$. Note that $E_r = E/(1-\nu^2)$ when the materials of the colliding bodies are identical ($E_1 = E_2 = E$ and $\nu_1 = \nu_2 = \nu$). In order to apply Eqs. (1) and (2) to the problem at hand, the following assumptions should be valid:

- the contact area is small compared to the geometry of the colliding bodies;
- the contact areas are perfectly smooth, so there is no friction between the colliding bodies;
- the material is isotropic and linearly elastic, so no plastic deformation occurs;
- the contact time is long enough to establish a quasi-static state.

It is to be noted that Eq. (1) still holds with significant deviation from these assumptions [10].

Contact model (1) can be refined by adding a hysteretic damping term, see [11], accounting for energy loss during collision. The inclusion of hysteretic damping alters Eq. (1) to

$$\begin{aligned} F &= K_{\text{Hertz}}\delta^{1.5}\left(1 + \frac{\mu}{K_{\text{Hertz}}}\dot{\delta}\right) \\ &= K_{\text{Hertz}}\delta^{1.5}\left[1 + \frac{3(1-e^2)}{4}\frac{\dot{\delta}}{\dot{\delta}^-}\right] \quad \text{for } \delta \geqslant 0, \end{aligned} \tag{3}$$

in which $e$ is the coefficient of restitution, a geometry and material dependent measure for energy dissipation. Moreover, $\dot{\delta}^-$ represents the velocity difference of the two colliding bodies at the beginning of the collision. In [12,13] other types of smooth impact descriptions are discussed.

The parameter $K_{\text{Hertz}}$ was determined experimentally ($K_{\text{Hertz}} = 2.1 \times 10^8\ \text{N/m}^{1.5}$). The coefficient of restitution $e$ is also estimated by means of experiments ($e = 0.5$). The fact that $e$ differs significantly from 1 indicates that restitution should be added to the model. Both $K_{\text{Hertz}}$ and $e$ are obtained as least-squares estimates in which the information from several collisions is accounted for. The underlying experiment

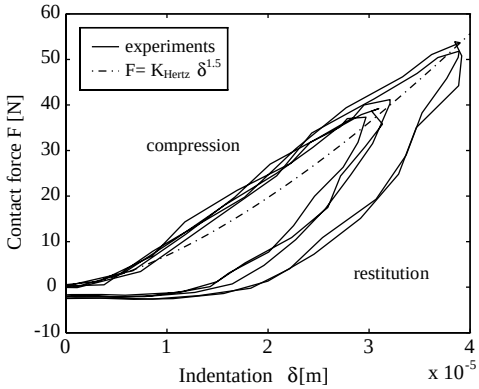


Fig. 3. Measurement of several collisions to estimate $K_{\mathrm{Hertz}}$ and $e$.

resulted in information regarding the indentation $\delta$, the indentation velocity $\dot{\delta}$, and the contact force $F$. The dependency of the contact force $F$ between the colliding half-spheres on the indentation $\delta$ is visualized in Fig. 3. The parameter $K_{\mathrm{Hertz}}$ can be estimated by comparing the contact force $F$ and the indentation $\delta$ at maximum indentation ($\dot{\delta}=0$), assuming that the static contact force is proportional to $\delta^{1.5}$, see Eq. (1). The coefficient of restitution $e$ can be estimated by considering the amount of energy loss $\Delta T$ during a collision. $\Delta T$ is equal to the surface within the hysteresis loop:

$$\Delta T = \oint \mu \delta^{1.5} \dot{\delta}\, \mathrm{d}\delta. \tag{4}$$

Therefore, $\mu$ can be estimated from

$$\mu = \frac{\Delta T}{\oint \delta^{1.5} \dot{\delta}\, \mathrm{d}\delta}. \tag{5}$$

The coefficient of restitution can now be obtained from

$$e = \sqrt{1 - \frac{\frac{4}{3}\mu \dot{\delta}^{-}}{K_{\mathrm{Hertz}}}}. \tag{6}$$

### 2.4. The non-linear dynamical model

In the previous two sections, the two components of the beam-impact system, namely, the beam and the elastic stop, were discussed. The assembled, non-linear model can be described by the following set of equations of motion:

$$\underline{M}\,\ddot{\underline{n}} + \underline{C}\,\dot{\underline{n}} + \underline{K}\,\underline{n} + \underline{K}_{\mathrm{H}}\varepsilon(\delta)\delta^{1.5}\left(1 + \frac{3(1-e^2)}{4}\frac{\dot{\delta}}{\dot{\delta}^{-}}\right) = \underline{m}_0 \ddot{y} \tag{7}$$

with

$$\epsilon(\delta) = \begin{cases} 1 & \text{for } \delta > 0, \\ 0 & \text{for } \delta \leqslant 0. \end{cases} \tag{8}$$

Herein, $\underline{n}$ is a two-dimensional column matrix of natural coordinates, which represent the contribution of the two modes to the total response, whereas $\underline{M}$ and $\underline{K}$ are the mass matrix and stiffness matrix, respectively, following from the Rayleigh–Ritz procedure. $\underline{C}$ represents the damping matrix which takes into account the measured modal damping (see Fig. 2). Moreover, $\underline{K}_{\mathrm{H}}$ is a coefficient matrix of the non-linearity while the term, in which $\underline{m}_0$ is involved, expresses the fact that the excitation is a prescribed displacement. Additionally, $\delta$ is the first component of $\underline{\delta} = [\delta, \delta_m]^{\mathrm{T}} := [y - x(z = l + l_{\mathrm{e}}/2),\ y - x(z = \frac{l}{2})]^{\mathrm{T}}$, representing the relative displacement of the beam with respect to the rigid frame at the point of contact of the two half-spheres. Note that $\underline{\delta}$ can be written as a linear combination of the components of $\underline{n}$. Moreover, in (7) $\dot{\delta}$ represents the relative velocity at the same point.

This model will now be used to simulate (through numerical time integration) the non-linear response $\underline{\delta}$ for different excitation forms $y = y(t)$. It should be noted that the magnitude of the elements in $\underline{K}_{\mathrm{H}}$ considerably exceeds that of those in $\underline{K}$. The system can, therefore, be considered to be strongly non-linear.

## 3. Survey of simulated response to periodic excitation

In order to enlarge the ability to interpret the stochastic response phenomena, to be discussed later on in this paper, we present some periodic response phenomena of the non-linear beam system. In Fig. 4, the maximum, absolute displacements $|\delta|_{\max}$ (of the periodic solutions) are plotted against the angular frequency $\omega_{\mathrm{e}}$ of the periodic (harmonic) base-excitation $y = y(t)$. These data were obtained using a periodic solver and a path-following procedure [1,3]. Some very important non-linear response characteristics can be extracted from Fig. 4. Firstly, besides

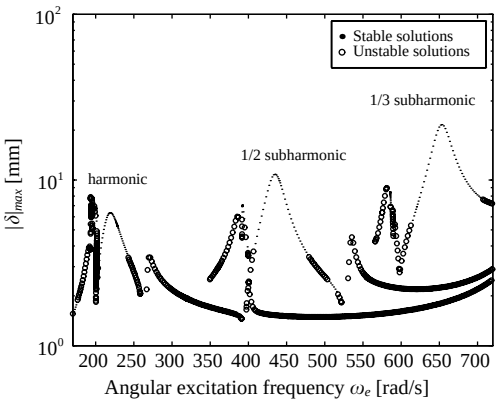


Fig. 4. Maximum, absolute displacements $|\delta|_{\max}$ of periodic solutions of the 2DOF beam-impact system.

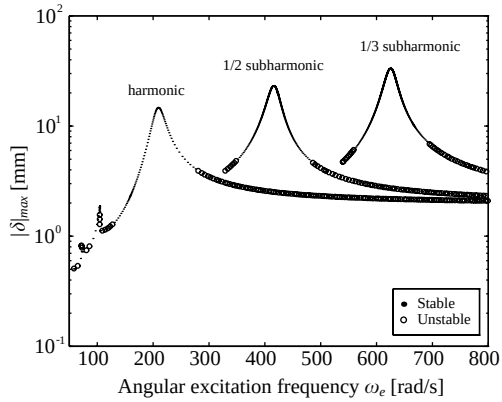


Fig. 5. Maximum, absolute displacements $|\delta|_{\max}$ of periodic solutions of the SDOF beam-impact system.

the harmonic resonance, corresponding to the first linear eigenmode of the elastic beam, related subharmonic resonances appear. It should be noted that the period time of a harmonic solution equals that of the excitation. Moreover, a harmonic solution consists of the frequencies $\omega_e, 2\omega_e, 3\omega_e, \ldots$ and so on. A $1/n$ subharmonic solution, however, comprises the frequencies $(1/n)\omega_e, (2/n)\omega_e, (3/n)\omega_e, \ldots$, where the response period is the $n$th multiple of the excitation period. Secondly, a remarkable feature can be found in the fact that the maximum absolute values of the subharmonic solutions are higher than those of the harmonic solutions. Finally, a striking characteristic is expressed by the fact that both the harmonic and the $\frac{1}{2}$ subharmonic resonance peak exhibit large dents near their resonance frequencies. In Fig. 5, it is shown that this effect is absent when the periodic response of an SDOF model [7] of the beam-impact system is investigated and that it is, therefore, most likely caused by the presence of the second mode in the model. Note in this respect that the second harmonic resonance frequency (780 rad/s) lies at four times the frequency at which the first harmonic resonance shows a dent (195 rad/s). This typically non-linear characteristic was also observed in experiments [14]. Clearly, the inclusion of extra 'modes' in the model not only affects the response in the neighbourhood of the resonance frequency of this 'mode', but also influences the response characteristics at lower frequencies dramatically.

## 4. Simulation approach for Gaussian excitation

### 4.1. Generation excitation signals

As mentioned before, the excitation form applied to the non-linear beam system is Gaussian, band-limited noise. Now, we would like to be able to generate realizations of such a Gaussian excitation process, which exhibits the desired power spectral density $S_{yy}(\omega)$. The energy of a band-limited, random process is concentrated in the frequency band $\omega_{\text{band}} = [\omega_{\min}, \omega_{\max}]$ (for both positive and negative frequencies). For any shape of the power spectral density of the Gaussian process, within that frequency band, one can simulate realizations of such a process using a method developed by Shinozuka and Yang [15,16]. The idea behind the method is that a one-dimensional Gaussian, random process $y(t)$ with zero mean and a one-sided power spectral density $S^o_{yy}(\omega)$, with

$$S^o_{yy}(\omega) = \begin{cases} 2S_{yy}(\omega) & \text{for } \omega > 0 \\ S_{yy}(\omega) & \text{for } \omega = 0 \\ 0 & \text{for } \omega < 0, \end{cases} \tag{9}$$

can be represented by a sum of cosine functions with a uniformly distributed random phase $\Phi$. A realization $\bar{y}(t)$ of $y(t)$ can be simulated by

$$\bar{y}(t) = \sqrt{\Delta\omega}\,\mathrm{Re}\{F(t)\}, \tag{10}$$

in which $\mathrm{Re}\{F(t)\}$ is the real part of $F(t)$ and

$$F(t) = \sum_{k=1}^{N} \{\sqrt{2S_{yy}^{o}(\omega_k)}\, \mathrm{e}^{\mathrm{i}\phi_k}\} \mathrm{e}^{\mathrm{i}\omega_k t} \tag{11}$$

is the finite complex Fourier transform of $\sqrt{2S_{yy}^{o}(\omega)} \times \mathrm{e}^{\mathrm{i}\phi}$, in which $\phi$ is a realization for $\Phi$, and $\Delta\omega = \omega_k - \omega_{k-1}$. The Fourier transform can be efficiently computed using the fast Fourier transform (FFT) algorithm.

Then, we can obtain a realization of the response process using the numerical integration techniques. Because the excitation $y(t)$ does not contain infinitely high frequencies (like white noise does), Eq. (7) is not a stochastic differential equation [17,18]. Therefore, classical integration techniques can be used to solve it numerically [7].

### 4.2. Numerical time integration

Numerical time integration is used to compute time series of the response $\delta(t)$. The computed realizations of the response can be used to estimate the invariant measures of the stationary solutions, such as statistical moments, probability density function and power spectral density. For non-stationary responses many computationally expensive simulations would have to be executed in order to ensure an accurate estimate of the invariant measures at each point in time. However, the necessity of a large number of records can be eliminated when the response is stationary, as is the case here. In this case, ergodicity with respect to a particular statistical moment can be assumed. This assumption allows the determination of the specific ensemble statistical moment by using its temporal counterpart.

The accuracy of the estimates of the stochastic invariants depends on the length of the time series used (corresponding to a statistical error on the estimate of the stochastic invariant) and the integration accuracy underlying the time series. Therefore, the efficiency of the integration technique is an important issue. Variable step size schemes, in which stability checks and accuracy checks are performed at each integration step, are rather inefficient for our purpose. Therefore, a constant step size, second-order Runge–Kutta scheme is used. Higher-order schemes do not improve the order of convergence, since higher-order derivatives of the function $\underline{f}(\underline{x}, \ddot{y}, t)$ in the state-space formulation of (7), where

$$\underline{f}(\underline{x}, \ddot{y}, t) = [\dot{n}_1 \quad \dot{n}_2 \quad \ddot{n}_1 \quad \ddot{n}_2]^{\mathrm{T}} := [\dot{x}_1 \quad \dot{x}_2 \quad \dot{x}_3 \quad \dot{x}_4]^{\mathrm{T}} = \begin{bmatrix} x_3 \\ x_4 \\ -\underline{M}^{-1}\left([\underline{K} \quad \underline{C}]\underline{x} + \underline{K}_{\mathrm{H}}\epsilon(\delta)(\delta)^{1.5} \left[1 + \frac{3(1-e^2)}{4}\frac{\dot{\delta}}{\dot{\delta}^-}\right] - \underline{m}_0\ddot{y}\right) \end{bmatrix}, \tag{12}$$

do not exist in the entire state space for systems with stops. Since explicit integration schemes are only conditionally stable, a minimum step size (that ensures stability) can be determined. Due to the major difference in stiffness between contact and non-contact situations, the minimal step sizes for these situations differ enormously. It would be very inefficient to choose one single constant step size based on contact situations. Therefore, two different stable step sizes are used. Consequently, the time of impact has to be determined accurately (and in a computationally efficient manner) to avoid entering contact with the large integration time step. For this purpose the Hénon method [19] is implemented within the integration routine.

### 4.3. The Hénon method

The Hénon method [19] is used to determine the time of impact. Here, the Hénon method means rearranging Eq. (12) without the non-linearities in such a way that $\delta$ becomes the independent variable whereas $t$ becomes one of the dependent variables. The non-linear part is superfluous, because the last time interval before the impact is observed. Recall that $\delta$ is a linear function of the components of $\underline{n}$. At the last time step before impact, this rearranged equation is integrated until $\delta = 0$. This integration step results in the known variables $t_{\mathsf{contact}}$, $\underline{x}(t_{\mathsf{contact}})$, for which holds $\delta(t_{\mathsf{contact}}) = 0$. Then, a switch is made to a small integration step size, for solving Eq. (12), continuing at $t_{\mathsf{contact}}$. When leaving contact, the integration routine switches back to the large integration time step.

## 5. Simulation results for Gaussian excitation

Here, the simulation results will be discussed. The excitations $y(t)$, applied to the model, are realizations

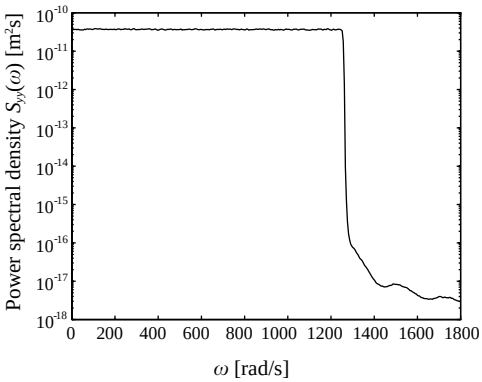


Fig. 6. Power spectral density of the excitation for $\omega_{\text{band}} = [0.0, 1226.6]$ rad/s.

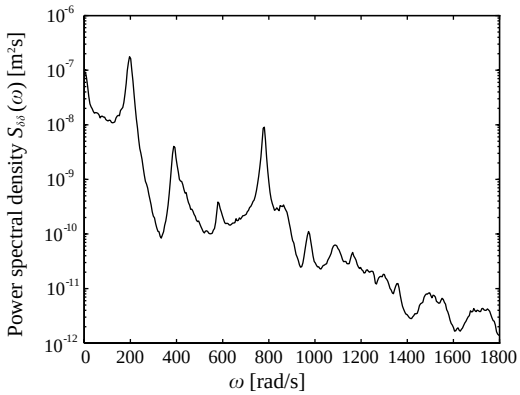


Fig. 7. Power spectral density of $\delta$ for $\omega_{\text{band}} = [0.0, 1226.6]$ rad/s.

of Gaussian, band-limited stochastic processes. The target spectrum[1] of the excitation is taken uniformly distributed within a limited frequency band $\omega_{\text{band}} = [\omega_{\min}, \omega_{\max}]$. First, a band excitation with $\omega_{\text{band}} = [0.0, 1226.6]$ rad/s is applied to the system. This excitation is broad-banded in relation to the response characteristics depicted in Fig. 4. In Fig. 6, the power spectral density of a base excitation $y$ is shown. It should be noted that the excitation is Gaussian by the nature of its generation. In Fig. 7, the power spectral density of the response variable $\delta$ is shown. The power spectral densities are estimated numerically using the Welch method [20]. The contribution of the

[1] It should be noted that for the remainder of this paper one-sided power spectral densities will be considered.

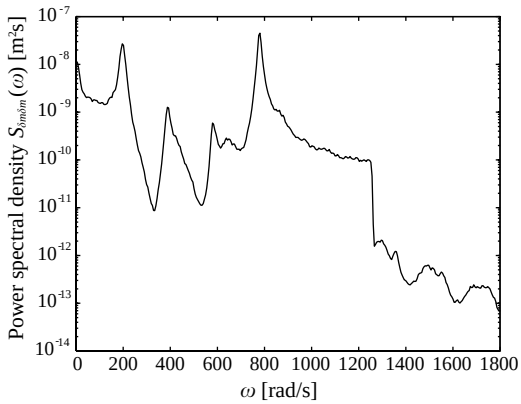


Fig. 8. Power spectral density of $\delta_m$ for $\omega_{\text{band}} = [0.0, 1226.6]$ rad/s.

first eigenmode is clearly present near $\omega = 195$ rad/s. The contribution of the second mode of the linear beam to $\delta$ is now apparent around $\omega = 780$ rad/s. Note that the first non-linear resonance frequency is almost twice the lowest linear eigenfrequency of the beam. In [21] is stated that in a piece-wise linear system the non-linear resonance frequency approaches twice the linear eigenfrequency (of the system without non-linearity) for a very high non-linearity. Since the impact phenomenon plays a less important role in the non-linear response related to the second mode, the second resonance frequency is much lower than twice the second linear eigenfrequency of the beam. The contribution of the second degree of freedom becomes more evident when one observes the power spectral density of the response variable $\delta_m$ for the same excitation, see Fig. 8. Herein, $\delta_m$ is the displacement of the beam relative to the rigid frame at a horizontal position $z = l/2$ on the beam (middle of the beam). The contribution of the second mode to the response of the system appears in a more dominant way in the mid-beam displacement (see Fig. 8), since the second mode has its maximum displacement near the middle of the beam. Note that, besides the resonances near 195 and 780 rad/s, extra (multiple) resonance peaks occur, which represent higher harmonics of the resonance near 195 rad/s (related to the first linear eigenmode of the elastic beam). Furthermore, the response signal contains a large amount of energy at low frequencies ($\omega < 50$ rad/s). The latter observation can be explained by the following reasoning. Due

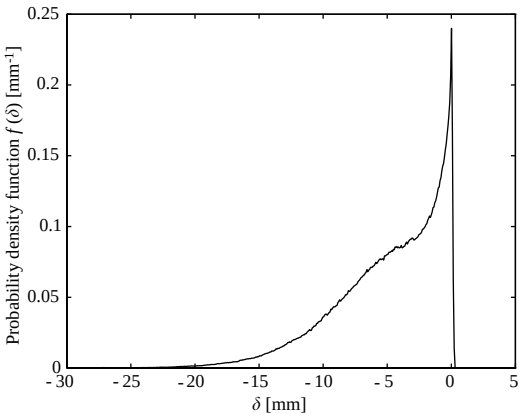


Fig. 9. Probability density function of $\delta$ for $\omega_{\text{band}} = [0.0, 1226.6]$ rad/s.

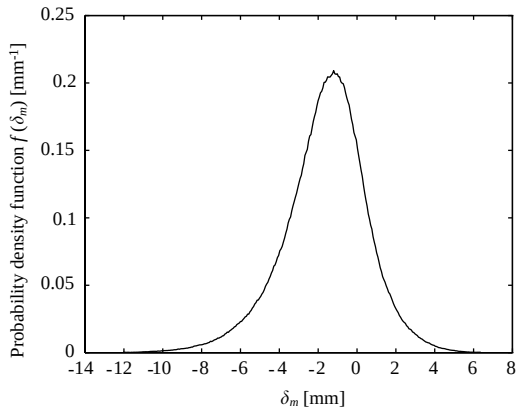


Fig. 10. Probability density function of $\delta_m$ for $\omega_{\text{band}} = [0.0, 1226.6]$ rad/s.

to the asymmetry of the non-linearity of the system, the frequencies in the response 'interact'. It is well known that when the excitation, and therefore the response, contains two frequencies $\omega_1$ and $\omega_2$, the response can also contain the frequency $\omega_2 - \omega_1$ when the system exhibits an asymmetric non-linearity. Note that the broad-banded excitation contains a large number of nearby frequencies. Hence, a lot of interaction can be expected in this case. When those excitation frequencies lie in a resonance peak of the system, these 'difference'-frequencies will contain a significant amount of energy. Both phenomena were also observed in the response of the SDOF model of the beam-impact system [5] and other non-linear systems with asymmetric stiffness non-linearities [7].

In Figs. 9 and 10, estimates for the probability density functions of the relative end-displacement $\delta$ and the relative mid-beam displacement $\delta_m$ are shown. Clearly, $\delta_m$ tends towards a Gaussian distribution. From a physical point of view, it is clear that $\delta_m$ should not exhibit such an extreme asymmetry as $\delta$, since the beam does not encounter a contact at the horizontal position $z = l/2$. Therefore, $\delta_m$ can become positive more easily than $\delta$. From a more general point of view, it is known [22] that the output of a linear system, in the case of a non-Gaussian input, will be closer to Gaussian than the input. In this perspective, we can view upon $\delta_m$ as an output of a linear system (the beam) with a non-Gaussian input $\delta$. This tendency towards a Gaussian distribution becomes stronger for weakly damped systems.

Next, three different narrow-band excitations were applied:

1. a band-limited excitation with $\omega_{\text{band}}=[144.5, 270.2]$ rad/s that covers the major part of the harmonic resonance peak, see Fig. 4;
2. a band-limited excitation with $\omega_{\text{band}}=[351.9, 477.5]$ rad/s that covers the major part of the $\frac{1}{2}$ subharmonic resonance peak, see Fig. 4;
3. a band-limited excitation with $\omega_{\text{band}}=[559.2, 684.9]$ rad/s that covers the major part of the $\frac{1}{3}$ subharmonic resonance peak, see Fig. 4.

It should be noted that all three excitation signals are realizations of Gaussian stochastic processes, which exhibit the same variance and have uniformly distributed energy within their specific frequency bands.

The power spectral densities of the responses to these excitations are displayed in the Figs. 11–13. Note that a 'harmonic' solution of the non-linear, 2DOF model to a harmonic excitation with frequency $\omega_e$ exists, see Fig. 4, and has a specific period time $2\pi/\omega_e$ but comprises multiple frequencies $\omega_e, 2\omega_e, 3\omega_e, \ldots$ . Clearly, this is also the case for stochastic excitations, see Fig. 11. Moreover, remarkable, stochastic, non-linear response phenomena are displayed in Figs. 12 and 13. Namely, Fig. 12 shows a 'stochastic $\frac{1}{2}$ subharmonic' solution and Fig. 13 shows a 'stochastic $\frac{1}{3}$ subharmonic' solution. Note that in the same frequency range subharmonic solutions exist when the system is excited periodically, see Fig. 4. To be more specific, a $1/n$ subharmonic effect is responsible for

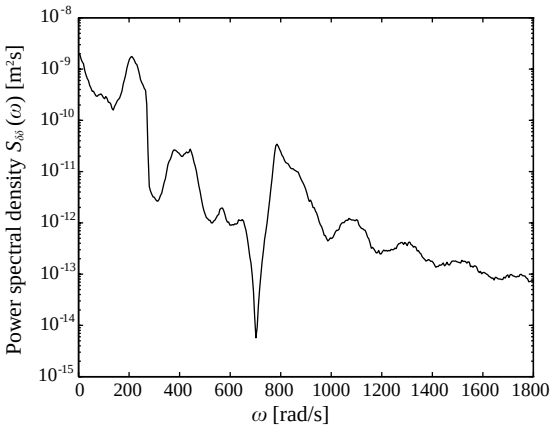


Fig. 11. Power spectral density of $\delta$ for $\omega_{\text{band}}=[144.5, 270.2]$ rad/s.

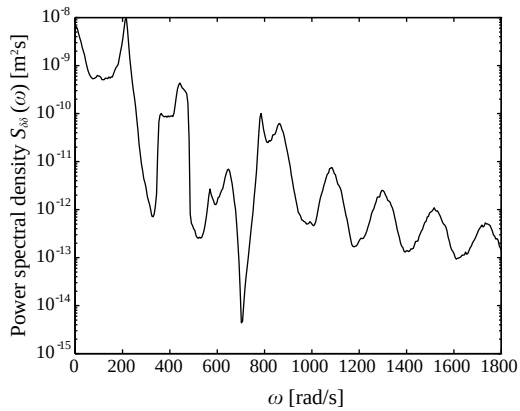


Fig. 12. Power spectral density of $\delta$ for $\omega_{\text{band}}=[351.9, 477.5]$ rad/s.

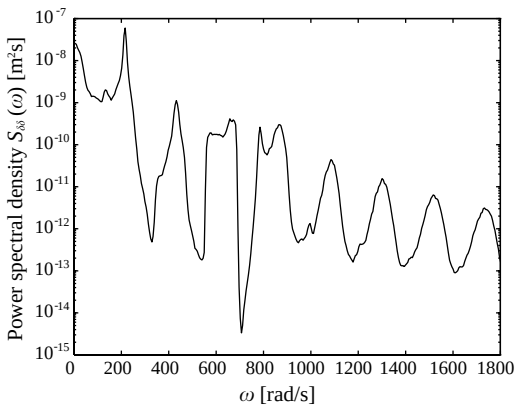


Fig. 13. Power spectral density of $\delta$ for $\omega_{\text{band}}=[559.2, 684.9]$ rad/s.

the fact that the excitation frequency band $[\omega_{\min}, \omega_{\max}]$ also results in an important response in the frequency range $[(\omega_{\min}/n), (\omega_{\max}/n)]$, see Figs. 12 and 13.

We can distinguish another, interesting, common characteristic of the periodic and stochastic response of the beam-impact system by comparing the Figs. 11–13. Namely, the 'stochastic $\frac{1}{3}$ subharmonic' solution contains significantly more energy than the 'stochastic $\frac{1}{2}$ subharmonic' solution, whereas the 'stochastic $\frac{1}{2}$ subharmonic' solution contains significantly more energy than the 'stochastic harmonic' solution. Note that a comparable phenomenon was observed in the periodic response of the MDOF model of the beam-impact system, see Fig. 4.

## 6. Experimental set-up

Several interesting, stochastic, non-linear response characteristics were observed in the previously discussed simulation results. In the next section, simulation results will be validated by comparison with experimental results. The experimental set-up is presented schematically in Fig. 14. A uniformly distributed, Gaussian, band-limited excitation signal is generated numerically using Shinozuka's method [15]. This signal is sent to a controller, which controls a servovalve using feedback information from an internal displacement transducer. The servovalve provides the input for the hydraulic actuator by controlling the oil flow of the hydraulic power supply. A hydraulic service manifold connects the hydraulic power supply and the servovalve. This service manifold reduces fluctuations and snapping in the hydraulic lines during dynamic programs. All measurements are monitored using the data acquisition software package DIFA [23].

Fig. 15 shows the measurement equipment mounted on the beam-impact system. A linear variable differential transformer (LVDT) measures the displacement of the rigid frame. The displacement and velocity of the beam, at the point of contact, are measured by a laser interferometer. Furthermore, the acceleration of the beam is measured by an accelerometer and a force transducer is used to measure the force acting on the rigid frame, where the force transducer is positioned at the centre of mass of the rigid frame and the rotations of the rigid frame are assumed to be small. The rigid

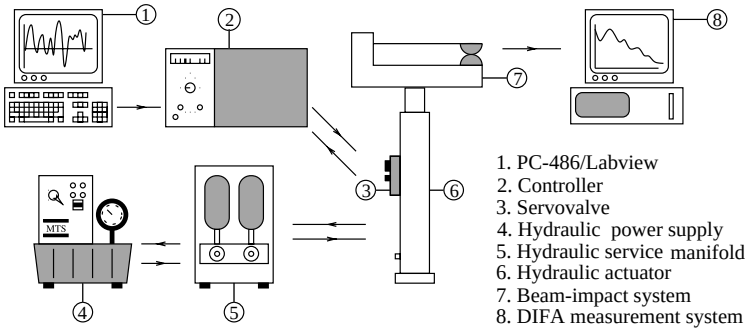


Fig. 14. The experimental set-up of the beam-impact system.

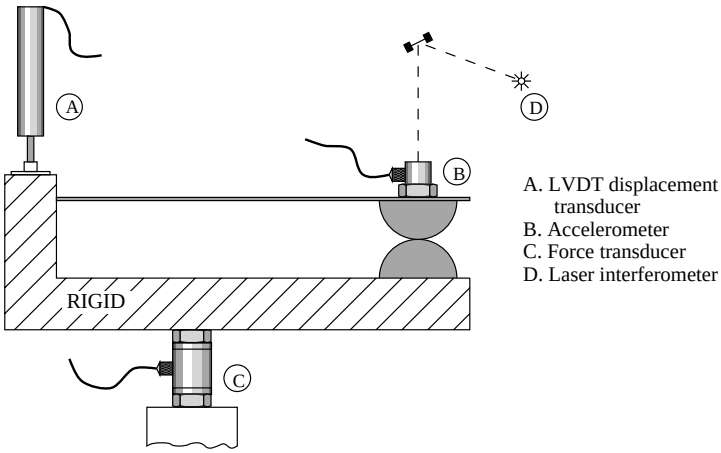


Fig. 15. The measurement equipment.

frame displacement measurements are used as input for the simulations described in the next section. Consequently, we can compare the results of these simulations to the experimental results.

## 7. Experimental results

In Section 5, several interesting, stochastic, non-linear response characteristics were observed in the simulation results. Comparable phenomena are encountered in the experiments as well and will be discussed here. Moreover, the validity of the 2DOF model will be assessed by comparing the experimental results with the simulation results. Here, also the added value of the 2DOF model with regard to the SDOF model, as presented in [5], can be assessed.

A $[0.0, 1226.6]$ rad/s band excitation was applied. The realized excitation spectrum is depicted in Fig. 16. In contrast to the signal offered to the controller, the power spectral density of the actual rigid frame displacement is clearly not uniformly distributed within the specified frequency range. This is due to the fact that the hydraulic actuator behaves like a first-order low-pass filter. Therefore, it is necessary to perform simulations with these rigid frame excitation spectra in order to be able to make appropriate comparisons between the results of the simulations and those of the experiments. Both the simulated and measured power spectral densities of the response $\delta(t)$ are shown in Fig. 17. The most important response phenomena like higher harmonics, related to the resonance near 195 rad/s, and the presence of a large amount of low-frequency energy are clearly

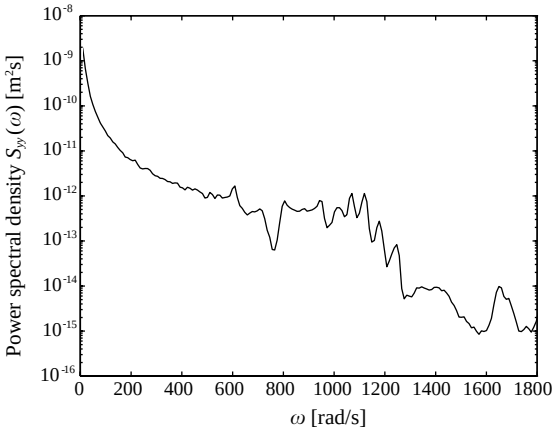


Fig. 16. Power spectral density of the excitation for $\omega_{\text{band}} = [0.0, 1226.6]$ rad/s.

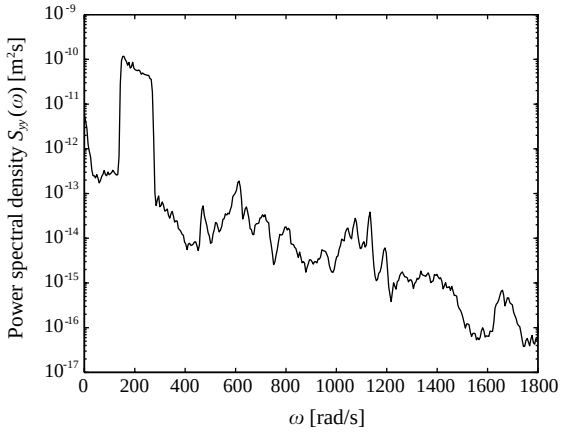


Fig. 18. Power spectral density of the excitation for $\omega_{\text{band}} = [144.5, 270.2]$ rad/s.

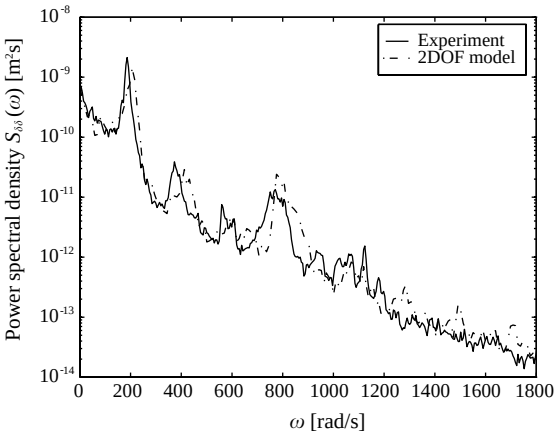


Fig. 17. Comparison of the power spectral densities of $\delta$ for the experiment and the 2DOF model with $\omega_{\text{band}} = [0.0, 1226.6]$ rad/s.

visible in both experimental and simulation results. However, the non-uniformity of $S_{yy}(\omega)$ obstructs the observation of the second characteristic. Fig. 17 shows that the experimental and numerical results correspond to a large extent. Clearly, the response of the 2DOF model exhibits the second harmonic resonance at $\omega = 780$ rad/s, which coincides with the experimental data. This represents an important modelling improvement in comparison with the SDOF model [5], since, obviously, the second mode is absent in the SDOF model.

In Fig. 19, the power spectral densities of the responses of the SDOF model and the 2DOF model for an 'experimental' $[144.5, 270.2]$ rad/s excitation (see Fig. 18) are compared.

This figure shows that the addition of the extra degree of freedom has a significant effect on the stochastic response of the system: this effect not only expresses itself through the second (stochastic) harmonic resonance peak near 780 rad/s, but also affects the response characteristics in lower frequency ranges. Fig. 20 shows that particularly this effect of the second degree of freedom makes the simulation results of the 2DOF model fit the experimental results better than the results of the SDOF model (observe, Figs. 19 and 20 simultaneously). The fact that the extension towards a 2DOF model also affects the response at lower frequencies corresponds to tendencies seen in the periodic response of the 2DOF model, see Fig. 4. However, for stochastic excitations the effect of the addition of the second degree of freedom does not seem to have such a dramatic effect on the response (at lower frequencies) as for periodic excitation. Apparently, local effects (in terms of frequency) are somehow averaged for stochastic excitations. Note, moreover, that the experimental data in Fig. 20 express the fact that a 'stochastic harmonic' response also appears in the experiment.

Fig. 22 displays an experimental 'stochastic $\frac{1}{2}$ subharmonic' solution, which occurs when the applied, Gaussian excitation exhibits a power spectral

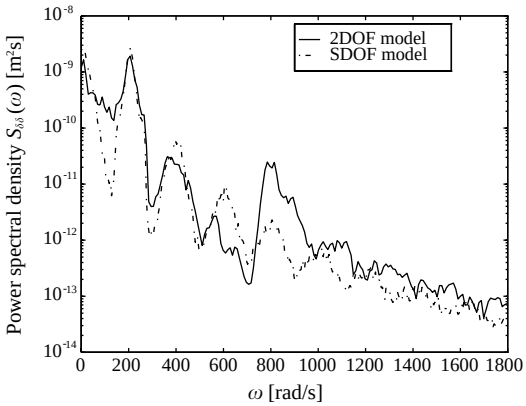


Fig. 19. $S_{\delta\delta}(\omega)$ for the SDOF model and the 2DOF model for $\omega_{\text{band}} = [144.5, 270.2]$ rad/s.

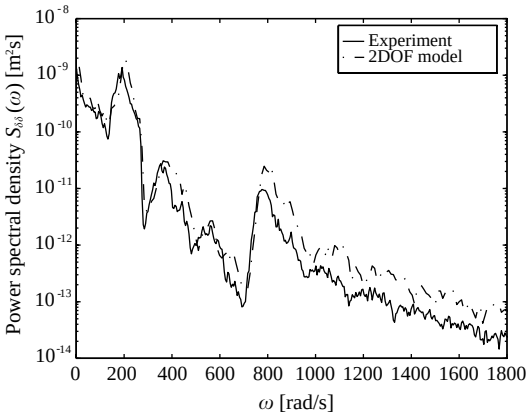


Fig. 20. $S_{\delta\delta}(\omega)$ for the experiment and the 2DOF model for $\omega_{\text{band}} = [144.5, 270.2]$ rad/s.

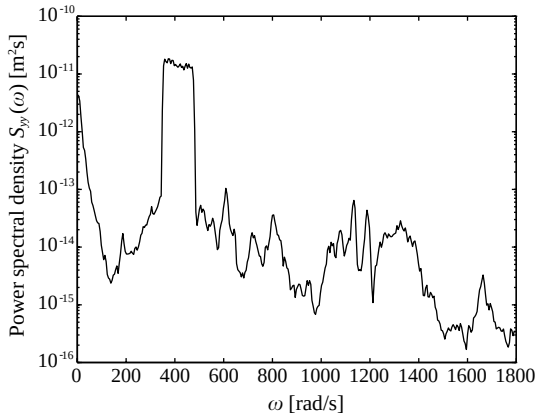


Fig. 21. Power spectral density of the excitation for $\omega_{\text{band}} = [351.9, 477.5]$ rad/s.

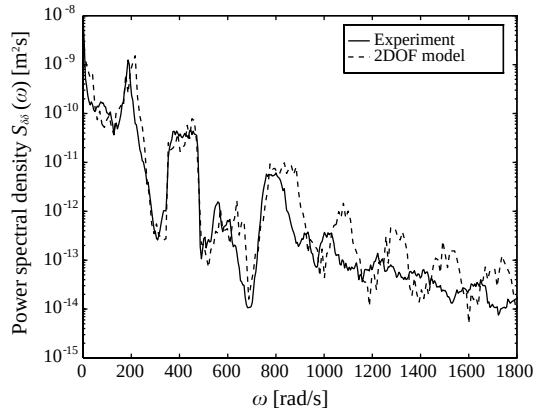


Fig. 22. $S_{\delta\delta}(\omega)$ for the experiment and the 2DOF model for $\omega_{\text{band}} = [351.9, 477.5]$ rad/s.

density as depicted in Fig. 21. Furthermore, Fig. 22 confirms once more that the 2DOF model describes all the important dynamic phenomena of the stochastic response of the experimental system very well.

Moreover, by comparing the Figs. 20 and 22 we can detect that the energy of both experimental stochastic solutions are of a comparable level. Note, however, that the power spectral density of the excitation in Fig. 21 is significantly lower than that in Fig. 18. So, this effect corresponds with an effect, which was also observed for the periodic and stochastic simulations, see Sections 3 and 5, respectively. There, the $\frac{1}{2}$ subharmonic solution proved to be of a higher energy level than the harmonic solution (for identical input levels).

## 8. Conclusions

We have investigated the stochastic response phenomena of a beam-impact system under band-limited, stochastic excitation both experimentally and numerically. Clearly, the simultaneous observation of the periodic and stochastic behaviour of the system proved to be very fruitful in gaining understanding with respect to the stochastic response phenomena. For a num-

ber of periodic response phenomena stochastic equivalents were presented, such as 'stochastic harmonic' and 'stochastic subharmonic' solutions. Here, it was of utmost importance to observe the response from a frequency-domain perspective.

Moreover, it was shown that the 2DOF model can predict the stochastic behaviour of the experimental system very accurately. Here, it is important to note that the addition of the second mode (near 780 rad/s) does not only result in a modelling improvement near this second resonance, but also accomplishes a significant improvement for lower frequencies, when compared to the SDOF model [5]. So, even for excitation spectra up to 500 rad/s, the 2DOF model should be preferred over the SDOF model. Moreover, an extension towards a 3DOF model will most probably not yield a better approximation of the experimental response characteristics, since, firstly, the 2DOF description is already very accurate for the frequency range observed in this paper. Moreover, the third mode (eigenfrequency is approximately 2300 rad/s) will become more important when one is interested in response characteristics in this 'higher' frequency range and when the excitation exhibits a significant amount of energy in this frequency range. Furthermore, an extension towards a model with more degrees-of-freedom will directly result in a decrease in computational efficiency, which is crucial in the numerical approximation of stochastic response charactertistics. It can, therefore, be concluded that the modelling approach, in which the continuous, linear part of the beam-impact system (the elastic beam) is reduced to a two-mode description before merging it with a model for the local non-linearity, is a valid and successful one for both periodic (see Ref. [1]) and stochastic excitations.

## References


[1] R.H.B. Fey, Steady-state behaviour of reduced dynamic systems with local nonlinearities, Ph.D. Thesis, Eindhoven University of Technology, The Netherlands, 1992.

[2] R.H.B. Fey, D.H. Van Campen, A. De Kraker, Long-term structural dynamics of mechanical systems with local nonlinearities, Trans. ASME, J. Vib. Acoust. 118 (2) (1996) 147–153, also publ. in: R.A. Ibrahim, N.S. Namachchivaya (Eds.), Proceedings of the Winter Annual Meeting ASME, Anaheim, CA, USA, 8–13 November, DE-Vol. 50, AMD-Vol. 44, 1992, pp. 159–167.

[3] E.L.B. Van de Vorst, Long-term dynamics and stabilization of nonlinear mechanical systems, Ph.D. Thesis, Eindhoven University of Technology, The Netherlands, 1996.

[4] D.H. Van Campen, A. De Kraker, R.H.B. Fey, E.L.B. Van de Vorst, J.A.W. Van der Spek, Long-term dynamics of nonlinear mdof engineering systems (Special issue on nonlinearities Mech. Eng.), Chaos Solitons Fract. 8 (4) (1997) 455–477.

[5] N. Van de Wouw, H.L.A. Van den Bosch, A. De Kraker, D.H. Van Campen, Experimental and numerical analysis of nonlinear phenomena in a stochastically excited beam system with impact, Chaos Solitons Fract. 9 (8) (1998) 1409–1428.

[6] L. Meirovitch, Principles and Techniques of Vibrations, Prentice-Hall International, New Jersey, 1997.

[7] N. Van de Wouw, Steady state behaviour of stochastically excited nonlinear dynamic systems, Ph.D. Thesis, Eindhoven University of Technology, 1999.

[8] H. Hertz, Gesammelte Werke, Vol. 1: Schriften Vermischten Inhalts, J.A. Barth, Leipzig, Germany, 1895 (in German).

[9] W. Goldsmith, Impact: the Theory and Physical Behaviour of Colliding Solids, E. Arnold Ltd., London, 1960.

[10] P.J.M. Roozen-Kroon, Structural optimization of bells, Ph.D. Thesis, Eindhoven University of Technology, The Netherlands, 1992.

[11] H.M. Lankarani, P.E. Nikravesh, Continuous contact force models for impact analysis in multibody systems, Nonlinear Dyn. 5 (1994) 193–207.

[12] K. Hunt, F. Crossley, Coefficient of restitution interpreted as damping in vibroimpact, ASME J. Appl. Mech. 97 (1975) 440–445.

[13] R. Ibrahim, M. El-Sayad, Simultaneous parametric and internal resonances in systems involving strong non-linearities, J. Sound Vib. 225 (5) (1999) 857–885.

[14] E. Van de Vorst, M. Heertjes, D. Van Campen, A. De Kraker, R. Fey, Experimental and numerical analysis of the steady-state behaviour of a beam system with impact, J. Sound Vib. 212 (2) (1998) 321–336.

[15] M. Shinozuka, Monte Carlo solution of structural dynamics, Comput. Struct. 2 (1972) 855–874.

[16] J.-N. Yang, Simulation of random envelope processes, J. Sound Vib. 21 (1) (1972) 73–85.

[17] L. Arnold, Stochastic Differential Equations: Theory and Applications, Wiley, New York, 1974.

[18] P.E. Kloeden, E. Platen, Numerical Solution of Stochastic Differential Equations, Springer, Berlin, 1992.

[19] M. Hénon, On the numerical computation of Poincaré maps, J. Appl. Mech. 47 (1982) 931–939.

[20] A.V. Oppenheim, R.W. Schafer, Digital Signal Processing, Prentice-Hall Inc., Englewood Cliffs, 1975.

[21] S.W. Shaw, P.J. Holmes, A periodically forced piecewise linear oscillator, J. Sound Vib. 90 (1) (1983) 129–155.

[22] J.B. Roberts, P.D. Spanos, Random Vibration and Statistical Linearization, Wiley, New York, 1990.

[23] DIFA, FA100 User Manual, DIFA Measuring Systems, Breda, The Netherlands, 1992.